PHOTONICS Research

Sensitivity-enhanced surface plasmon resonance sensor utilizing a tungsten disulfide (WS₂) nanosheets overlayer

Hao Wang,[1,†] Hui Zhang,[1,4,†] Jiangli Dong,[1,2] Shiqi Hu,[1] Wenguo Zhu,[3] ⓘ Wentao Qiu,[3] Huihui Lu,[1] Jianhui Yu,[1,3] Heyuan Guan,[1,3] Shecheng Gao,[2] Zhaohui Li,[1,5] Weiping Liu,[2] Miao He,[4] Jun Zhang,[1] Zhe Chen,[1,3] and Yunhan Luo[1,2,3,*]

[1]*Guangdong Provincial Key Laboratory of Optical Fiber Sensing and Communications, Jinan University, Guangzhou 510632, China*
[2]*Key Laboratory of Optoelectronic Information and Sensing Technologies of Guangdong Higher Education Institutes, Jinan University, Guangzhou 510632, China*
[3]*Key Laboratory of Visible Light Communications of Guangzhou, Jinan University, Guangzhou 510632, China*
[4]*School of Physics and Optoelectronic Engineering, Guangdong University of Technology, Guangzhou 510006, China*
[5]*State Key Laboratory of Optoelectronic Materials and Technologies and School of Electronics and Information Technology, Sun Yat-sen University, Guangzhou 510275, China*
*Corresponding author: yunhanluo@163.com

Tungsten disulfide (WS₂), as a representative layered transition metal dichalcogenide (TMDC) material, possesses important potential for applications in highly sensitive sensors. Here, a sensitivity-enhanced surface plasmon resonance (SPR) sensor with a metal film modified by an overlayer of WS₂ nanosheets is proposed and demonstrated. The SPR sensitivity is related to the thickness of the WS₂ overlayer, which can be tailored by coating a WS₂ ethanol suspension with different concentrations or by the number of times of repeated post-coating. Benefitting from its large surface area, high refractive index, and unique optoelectronic properties, the WS₂ nanosheet overlayer coated on the gold film significantly improves the sensing sensitivity. The highest sensitivity (up to 2459.3 nm/RIU) in the experiment is achieved by coating the WS₂ suspension once. Compared to the case without a WS₂ overlayer, this result shows a sensitivity enhancement of 26.6%. The influence of the WS₂ nanosheet overlayer on the sensing performance improvement is analyzed and discussed. Moreover, the proposed WS₂ SPR sensor has a linear correlation coefficient of 99.76% in refractive index range of 1.333 to 1.360. Besides sensitivity enhancement, the WS₂ nanosheet overlayer is able to show additional advantages, such as protection of metal film from oxidation, tunability of the resonance wavelength region, biocompatibility, capability of vapor, and gas sensing.   © 2018 Chinese Laser Press

OCIS codes: (250.5403) Plasmonics; (240.6690) Surface waves; (280.4788) Optical sensing and sensors.

https://doi.org/10.1364/PRJ.6.000485

1. INTRODUCTION

In recent years, there have been dramatically increasing concerns among various disciplines on two-dimensional transition metal dichalcogenides (TMDCs) [1], such as molybdenum disulfide (MoS₂) [2] and tungsten disulfide (WS₂) [3], due to their atomically thin layered structures with unique electrical, optical, plasmonic, electrochemical, and electrocatalytic properties [4–7]. WS₂ possesses a hexagonal crystal structure formed by a covalently attached S-W-S monolayer and stacked through weak van der Waals force [8]. A WS₂ monolayer contains one layer of tungsten atoms with sixfold coordination symmetry, which are hexagonally packed between two trigonal

atomic layers of sulfur atoms. Hence, WS₂, as one of the newly emerging 2D layered nanomaterials, is considered as a graphene-like material [9]. There are a number of techniques for TMDC synthesis, such as chemical vapor deposition, mechanical exfoliation, and the liquid phase exfoliation method [10]. As a typical kind of TMDC material, WS₂ possesses strong photoluminescence, large photoresponsivity, high density of electronic states, sizable band gaps in the visible to near-infrared spectrum, and high surface-to-volume and layer-dependent electronic and optical properties, making it a promising material for offering numerous opportunities in the development of new biological and chemical sensors and

sensing strategies [11]. For instance, it has been reported that the plasma-assisted synthesis of WS_2 thin films exhibits high sensitivity to the presence of NH_3, which demonstrates the potential of 2D WS_2 films for electrochemical gas sensing applications [12]. A new WS_2 nanosheet-based nanosensor for the ultrasensitive detection of small molecule–protein receptor interaction has been reported, which exhibits high sensitivity with a detection limit of 5.3 pmol/L [13]. Wrapped on the tapered region of microfiber, WS_2 nanosheets have been proposed for enhanced humidity sensing [14].

Surface plasmon resonance (SPR) is an exceedingly efficient and powerful technique for real-time and label-free biomolecular interactions and chemical analyte detection via monitoring refractive-index changes of the surrounding medium at the SPR sensing surfaces due to its strong evanescent field with a penetration depth for tens to hundreds of nanometers [15,16]. However, the SPR sensors usually show insufficient ability in the direct detection of small molecular weight molecules, extremely dilute concentration of analytes, or low-affinity interactions [17,18]. To overcome this limitation of SPR sensors, many sensitivity-enhancement schemes have been proposed, for example, combining the strong electric field of localized SPR excitation based on noble-metal plasmonic nanoparticles (e.g., Au and Ag nanoparticles) [19,20], employing functionalized magnetic nanoparticles as SPR signal amplification tags [21], or enhancing the SPR sensing substrate by depositing on the metal film with an additional layer of modified materials. Some common modified materials have been reported, such as a nanometer layer of Si film [22], various high-index oxide overlayers (Al_2O_3, SnO_2, TeO_2, MgO, ITO, and ZnO) [23,24], and a few-nanometers-thick layer of amorphous silicon-carbon alloy [25]. In addition, a 2D layered nanomaterial, graphene, has been widely investigated and reported in the aspect of enhancing performance and sensitivity of SPR-based sensors owing to the significant advantages of graphene functionalized SPR surfaces [26–28]. As a graphene-like material, WS_2 nanosheets also possess the properties of 2D layered nanomaterials, like chemical stability, large surface area, and high refractive index, to play efficient roles in the sensitivity enhancement for the optical sensors. An SPR biosensor based on a gold/Si/WS_2 hybrid nanostructure has been theoretically designed and proposed to investigate the sensing performance improvement [29]. But the ability of WS_2 nanosheets in enhancing the sensitivity and selectivity of SPR-based sensors has been little investigated experimentally.

In this work, WS_2 nanosheets were experimentally introduced to the SPR sensor by coating onto the gold film to explore the scheme for sensing performance improvement. The influence of WS_2 overlayers with different thicknesses on the refractive index (RI) sensing sensitivity was studied and discussed in detail. Different thicknesses of WS_2 overlayer were obtained by different number of times performing the post-coating process. With the increase of the WS_2 overlayer thickness, the sensing sensitivity increases first and then decreases. The highest sensitivity (up to 2459.3 nm/RIU) is experimentally achieved at one post-coating of the WS_2 suspension. Compared to the case of the uncoated SPR sensor, it shows a sensitivity enhancement of 26.6%. The effect of the WS_2 overlayer on sensitivity enhancement is discussed and explained. To the best of our knowledge, this is the first report on utilization of WS_2 nanosheets in SPR-based sensor to enhance the RI sensing sensitivity.

2. FABRICATION AND CHARACTERIZATION

The proposed SPR sensor is based on the conventional Kretschmann attenuated total reflection (ATR) structure with a custom-built glass slide as the metal deposition substrate to make the prism be used repeatedly. Firstly, glass slides were cleaned by immersing into an ultrasonic bath for 10 min. In the subsequent metal deposition process, a thin layer (~5 nm) of chromium and a gold film (50 nm) were successively deposited onto the slides by a vacuum evaporating method, wherein the chromium layer was applied to enhance the adhesion force between the glass slide and the gold film. The final step is to coat the prepared WS_2 alcohol suspension onto the gold film and form a WS_2 modified SPR chip.

The WS_2 alcohol suspension (WS_2 nanosheet concentration is 1 mg/mL, average nanosheet size is 20–200 nm) used in the experiment was purchased from MKNANO Tec. Co., Ltd. The WS_2 alcohol suspension was decanted into centrifuge tube and treated by ultrasonication for 30 min with the purpose of distributing the WS_2 nanosheets to avoid agglomeration. After that, the suspension was dropped directly onto the gold film surface and placed at room temperature for ~10 h to evaporate the alcohol naturally. As a result, a certain thickness of WS_2 film could firmly attach on the gold layer. Raman scattering spectroscopy of the WS_2 overlayer on the gold film was performed to characterize its thickness and structural quality. The Raman spectrum excited by a laser at wavelength 514.5 nm was measured with a Raman microscope (RENISHAW, UK) and depicted in Fig. 1. The 2LA (M) and A_{1g} (Γ) peak positions are at 353 cm^{-1} and 418.3 cm^{-1}, respectively. According to Ref. [30], the number of WS_2 nanosheet layers can be nondestructively analyzed by observing the shifts in these Raman mode peaks. By comparing the intensity ratios and peak frequencies of the WS_2 Raman modes in Fig. 1 with those in Ref. [30], the WS_2 nanosheets constituting the WS_2 overlayer coated on the gold film can be estimated to be multilayer.
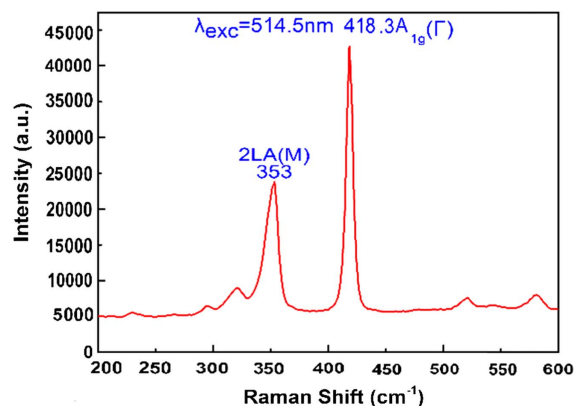

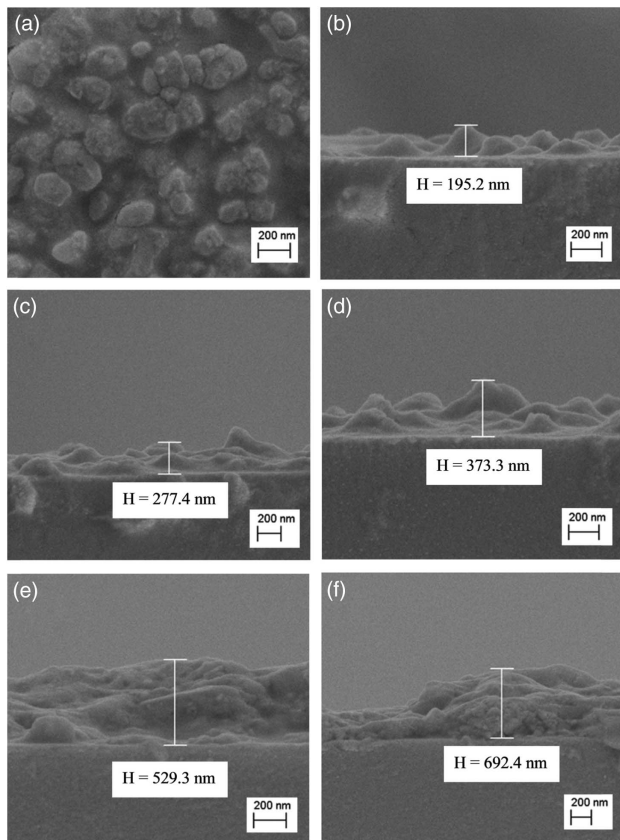**Fig. 1.** Raman spectrum of the WS_2 layers on the SPR sensor structure.

Fig. 2. (a) WS$_2$ surface morphology image of the SPR sensor. The WS$_2$ cross section SEM images after different numbers of times of repeated post-coating: (b) one; (c) two; (d) three; (e) four; (f) five.

Fig. 3. Experimental setup for RI sensing measurement.

The WS$_2$ nanosheet on the outside surface layer of the substrate plays a key role in the eventual RI sensing experiment.

To obtain the surface morphology and the thickness of the WS$_2$ overlayer coated on the gold film with different number of times of post-coating, the sensors were observed with a scanning electron microscope (SEM). The thickness can be increased by repeated post-coating. Figure 2(a) shows the SEM image of WS$_2$ surface morphology on the SPR sensor at a magnification of 29330. It can be seen that the WS$_2$ nanosheets nearly uniformly distribute on the gold film. Figures 2(b)–2(f) provide the WS$_2$ cross-section SEM images after different number of times of post-coating. The experimental observation results indicate that the thicknesses of the WS$_2$ overlayer are 195.2, 277.4, 373.3, 529.3, and 692.4 nm for the one to five times of post-coating, respectively. The thickness of WS$_2$ overlayer has a significant influence on the sensing property, which can be illustrated in the latter RI sensing experimental results.

3. SENSOR PERFORMANCE MEASUREMENT

All the SPR spectra were measured via coupling the tungsten-halogen light source [AvaLight-HAL-(S)-Mini, China] to the Krestchmann configuration SPR system based on a prism and recording the reflected light with a spectrometer (AvaSpec-ULS2048XL, China). The specific experimental setup for
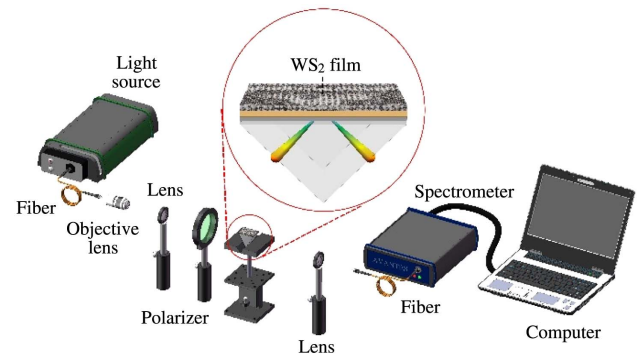
sensing measurement was constructed and shown in Fig. 3. The broadband signal light was transmitted through a fiber jumper from the tungsten-halogen source, focused and collimated by an objective lens and a plano-convex lens, polarized by a polarizer to obtain a transverse-magnetic light injection, and then coupled to the prism with the SPR excited by the evanescent wave at a certain wavelength. After that, the residual reflection light with a resonance dip was focused by a plano-convex lens and collected by a fiber spectrometer. Finally, the corresponding reflectance spectrum was recorded by a computer. The integration time is 3.6 ms, and the average times are 10. A WS$_2$-SPR chip was mounted on the top of the prism with a layer of oil applied for index matching. When the SPR was excited, a part of signal light was coupled into the surface plasmon wave. In consequence, a resonant absorption dip could be observed in the reflectance spectra, and the dip corresponds to the position of the resonance wavelength. Furthermore, due to the high sensitivity of SPR to surrounding refractive index, a change in the refractive index of the sensing medium on the surface of the WS$_2$ film would give rise to the resonance wavelength shift. The sensing performance of the WS$_2$-SPR sensor could be characterized in virtue of the shift amount.

In the experiment, solutions with different refractive indices were used as the RI sensing analytes. The solutions were obtained by mixing ethylene glycol and distilled water at a certain volume ratio. Their refractive indices were further measured with an Abbe refractometer (Edmund NT52-975, Edmund Optics Co., Ltd.) at room temperature of 25°C. Five solutions with the refractive indices of 1.333, 1.339, 1.344, 1.355, and 1.360 were prepared for the following RI sensing measurement experiment. At first, the RI sensing measurements of the SPR-based chip without a WS$_2$ nanosheet overlayer were carried out as the control group, and the corresponding reflectance spectra are shown in Fig. 4(a). It is clearly seen that all the reflectance spectra exhibit obvious SPR absorption dips. With the increase of analyte RI, the resonance dips shift to longer wavelengths. In the range of analyte RI changing from 1.333 to 1.360, the resonance wavelength redshifted 51.7 nm.

Figures 4(b)–4(f) provide the reflectance spectra of the WS$_2$-SPR sensor in the cases of being covered with different thicknesses of WS$_2$ nanosheet overlayer. In contrast to the control group, they also exhibit obvious SPR absorption dips, and the resonance dips also shift to the longer wavelengths with the
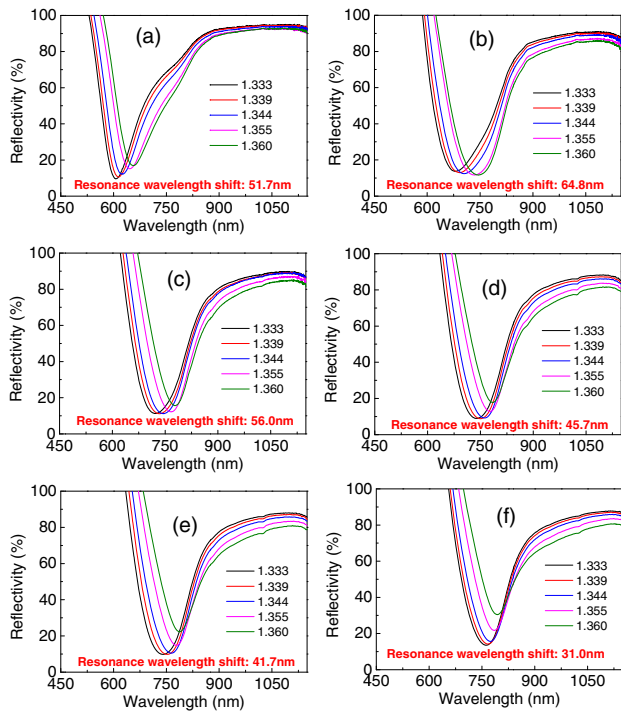
Fig. 4. Reflectance spectra of the WS_2-SPR sensors corresponding to different post-coating times: (a) Without coating; (b) one; (c) two; (d) three; (e) four; (f) five. The refractive index of the sensing analyte changes from 1.333 to 1.360.

Fig. 5. Experimental variation of shift in the resonance wavelength with refractive index under different times of WS_2 nanosheet post-coating: (a) Without coating; (b) one; (c) two; (d) three; (e) four; (f) five.

analyte RI increase. However, the resonance wavelength position displayed different shift amounts in the cases of different WS_2 nanosheet overlayer thicknesses. The resonance wavelength position shifted 64.8, 56.0, 45.7, 41.8, and 31.0 nm for the WS_2-SPR sensors coated with WS_2 nanosheets for one to five times, respectively. In addition, the SPR dips obviously broadened with the increased thickness of WS_2 overlay, which can be characterized by the full width at half-maximum (FWHM).

In order to describe the sensing performance more intuitively, the resonant wavelengths were plotted as the functions of the sensing refractive index for different times of WS_2 nanosheet suspension post-coatings in Figs. 5(a)–5(f), and the linear fittings were implemented to indicate the change trend of the resonant wavelength with sensing RI. As a result, the linearly dependent coefficients R^2 were 0.9924, 0.9976, 0.9974, 0.9895, 0.9881, and 0.9869 corresponding to the cases of zero to five times of WS_2 nanosheet coatings, respectively. These results adequately reveal that there is an excellent linear relationship between the resonant wavelength shifts and sensing RI changes. Thus, the sensing RI change can be detected through observing the resonance wavelength shifts.

Actually, the slopes of the fitted lines in Fig. 5 are the RI sensitivities for the sensors [31]. Therefore, the sensing sensitivities for zero to five times of WS_2 nanosheets coatings are 1942.2, 2459.3, 2073.4, 1677.6, 1515.9, and 1139.8 nm/RIU, respectively, and they were further plotted versus the different times of WS_2 nanosheet coatings in Fig. 6(a). It can be found that the sensitivity increases first
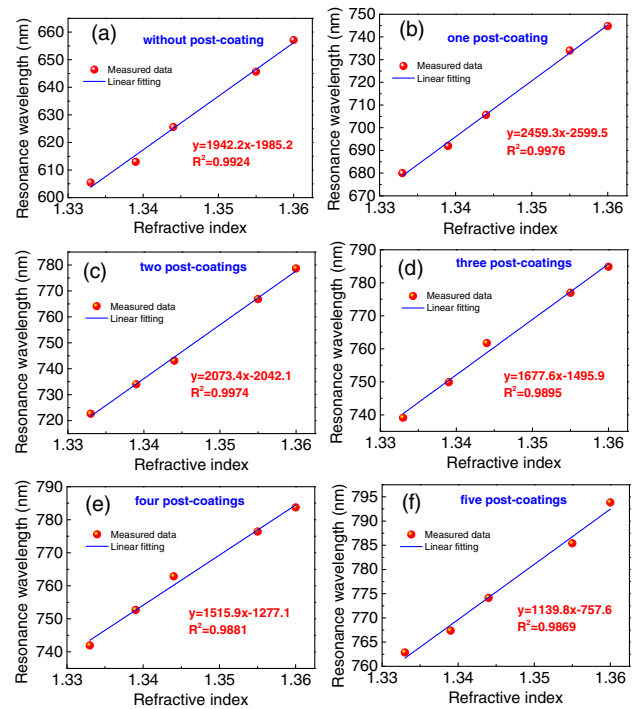
and then decreases with the increase of post-coating times. In the cases of one and two times of coatings, the sensitivities were improved obviously, compared to that without a WS_2 nanosheet overlayer. After post-coating once, the sensitivity is enhanced to 2459.3 nm/RIU, which is 26.6% more than the case without a WS_2 nanosheet overlayer.

Apart from the sensing sensitivity, the figure of merit (FoM), defined as the ratio between sensitivity and FWHM, is also a typical quality parameter for accessing the performance of SPR sensors. Figure 6(b) depicts the FoM variation as a function of the number of times of WS_2 nanosheet coating. Here, the FWHM of the SPR spectra for the analyte refractive index 1.333 in Fig. 4 was used to acquire the corresponding FoM. From Fig. 6(b), it can be seen that the FoM decreases with the increase of WS_2 nanosheet post-coating times. Compared with the case of uncoated gold film, a larger number of WS_2 nanosheets stacked on the gold film cause strong absorption
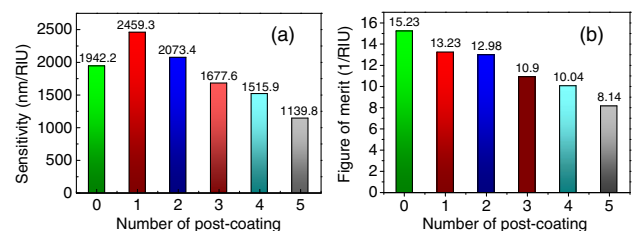

Fig. 6. (a) Sensitivity and (b) figure of merit comparison for different number of times of WS_2 nanosheets coatings.

and scattering, broaden the SPR dips, and thus result in the decrease of FoM.

4. ANALYSIS AND EXPLANATION

Since all the SPR sensors were prepared in the same way except the number of times of WS_2 post-coating, this suggests that the analysis could be carried out by treating the WS_2 and the analyte as a hybrid sensing layer. The introduction of the WS_2 will change the effective refractive index of the hybrid media and the evanescent field distribution as well.

First, we experimentally measured the SPR spectra of the sensor with uncoated gold film in the analyte refractive index range of 1.333 to 1.40 to observe the influence of the effective refractive index on the SPR sensitivity and plotted them in Fig. 7(a). The corresponding quadratic fitting curve with the dependent coefficient $R^2 = 0.9996$ for the resonance wavelength versus refractive index was depicted in Fig. 7(a). It can be found that the slope of the curve representing the sensor sensitivity in the different refractive index ranges increases with the increased refractive index. This means that the same refractive index increment in the high-refractive-index range will cause more resonance wavelength shift amount than that in the low-refractive-index range.

By means of post-coating, a mass of hollowness exists in the WS_2 nanosheet overlayer, which can be seen from the WS_2 overlayer SEM images shown in Fig. 2. Thereby, the introduction of additional WS_2 nanosheet overlayers with a high refractive index onto the gold film actually changes the sensing layer into the hybrid media of the analyte and WS_2 nanosheets. The corresponding effective refractive index can be expressed as $n_{eff} = f_{analyte} \times n_{analyte} + f_{WS2} \times n_{WS2}$, where $f_{analyte} = V_{analyte}/(V_{analyte} + V_{WS2})$ and $f_{WS2} = V_{WS2}/(V_{analyte} + V_{WS2})$ are the volume fractions of the analyte and WS_2 nanosheets, respectively, $V_{analyte}$ and V_{WS2} are the volumes of analyte and WS_2 nanosheets in the hybrid sensing layer, and $n_{analyte}$ and n_{WS2} are the refractive index for the analyte and WS_2 nanosheets in the sensing layer, respectively. It is apparent that one effect of the WS_2 overlayer is to change the volume fraction of analyte $f_{analyte}$. In the sensing experiment, the sensitivity of the sensor is calculated via $S = \Delta\lambda/\Delta n_{analyte}$; here $\Delta\lambda$ is the resonance wavelength shift amount and $\Delta n_{analyte}$ is the refractive index increment of the sensing analyte and is fixed at a value of 0.027 in the sensing measurement for the sensors with different WS_2 nanosheet overlayer thicknesses.

With the increase of WS_2 overlayer thickness, f_{WS2} increases, while $f_{analyte}$ decreases, which results in the decrease of the sensing effective refractive index increment $\Delta n_{eff} = f_{analyte} \times \Delta n_{analyte}$. Despite the decreased Δn_{eff}, the corresponding resonance wavelength shift amount $\Delta\lambda$ may increase due to the large slope in a region of the correlation curve. For visual demonstration, the segments in the quadratic fitting curve represent the resonance wavelength shift amounts for different number of times of WS_2 post-coating, and the corresponding effective refractive index increments were sectioned via different color dash lines, as shown in Fig. 7(a). The subscript numbers 0, 1, 2, and 5 represent the corresponding number of post-coating times. It can be seen that, although $\Delta n_{eff1} < \Delta n_{eff0}$, respectively, the corresponding resonance wavelength shift amount satisfies $\Delta\lambda_1 > \Delta\lambda_0$, which means that the sensitivity increases with an increase of WS_2 nanosheet overlayer thickness. However, this trend does not remain constant.

Another effect of the introduced WS_2 overlayer reflects in affecting the evanescent field distribution. The evanescent electric field distribution at the resonance wavelength within the prism/gold film (50 nm)/analyte ($n = 1.36$) structure was numerically calculated and illustrated in Fig. 7(b). Coating gold film with the WS_2 nanosheet overlayer will affect the evanescent electric field distribution, which in turn has an impact on the decay length. However, the precise field distribution corresponding to the WS_2-coated sensor is unavailable because of the lack of reported data for the optical constants in a broad spectral range for WS_2 material with a thickness of several hundred nanometers. Based on the fact that the decay length of the SPR evanescent field in the dielectric layer usually ranges from tens to hundreds of nanometers [15], the interaction strength between the evanescent field and the analyte will further decrease with the WS_2 overlayer thickness increasing and finally result in the decrease of the resonance wavelength shift amount $\Delta\lambda_2$. That is to say, the sensitivity goes into the decreasing trend after the WS_2 overlayer thickness beyond a critical value. For example, the resonance wavelength shift ($\Delta\lambda_5$) for five times of post-coating of the sensor is even smaller than that ($\Delta\lambda_0$) of the uncoated one.

Summarizing the two effects on the SPR sensitivity brought by the WS_2 nanosheet overlayer, positive enhancement and negative weakening due to different mechanisms exist simultaneously. Therefore, the experimental results for the sensitivity increasing first and then decreasing with the increase of WS_2 nanosheet overlayer thickness can be easily explained by the balance of the two abovementioned effects. As expected, a higher sensing performance can even be further improved by replacing the gold film with gold-silicon bilayer and reducing the thin WS_2 overlayer to several WS_2 nanosheet monolayers [29]. For the synthesis and deposition of a few layers of even monolayer of 2D materials, a liquid metal–based reaction technique may be referred to [32,33].

5. CONCLUSION

We have demonstrated the RI sensing sensitivity enhancement of SPR sensor by first introducing a layer of post-coating onto the gold film surface with a 2D layered nanomaterial, WS_2 nanosheets. The sensitivity is related to the thicknesses of
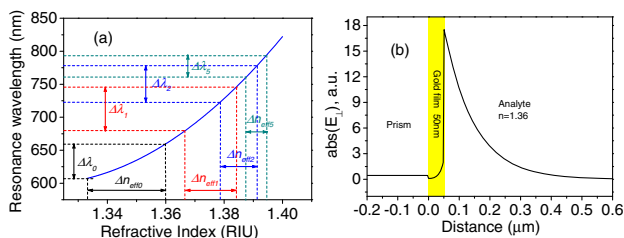
Fig. 7. (a) Experimental variation of shift in the resonance wavelength with surrounding refractive index ranging from 1.333 to 1.40. (b) Evanescent electric field distribution at the resonance wavelength within the prism/gold film (50 nm)/analyte ($n = 1.36$) structure.

the WS$_2$ nanosheet overlayer, which can be tailored by the number of post-coating times of a WS$_2$ ethanol suspension. With the increase of WS$_2$ nanosheet thickness, the sensing sensitivity increases first and then decreases, for which a detailed explanation is presented. The highest sensitivity (up to 2459.3 nm/RIU) is achieved in the case of a one-time post-coating of WS$_2$ nanosheets on the gold film in the experiment. Compared to the case of an uncoated sensor, the experimental result indicates that the presence of the WS$_2$ nanosheets coating results in an enhancement of 26.6% in sensitivity. Moreover, the proposed SPR sensor has a linear correlation coefficient of 99.76% in the refractive index range of 1.333 to 1.360. By means of a simple post-coating process, this work demonstrated an effective strategy to improve the sensor performance in term of sensing sensitivity. It is worth pointing out that the proposed WS$_2$ modified SPR sensors could hold considerable potential in biochemical detections by further exploiting the additional advantages of WS$_2$, such as large surface area and abundant surface functional groups.

†These authors contributed equally to this work.

REFERENCES

1. M. Chhowalla, H. S. Shin, G. Eda, L. J. Li, K. P. Loh, and H. Zhang, "The chemistry of two-dimensional layered transition metal dichalcogenide nanosheets," Nat. Chem. **5**, 263–275 (2013).
2. D. S. Tsai, K. K. Liu, D. H. Lien, M. L. Tsai, C. F. Kang, C. A. Lin, C. Lin, L. J. Li, and J. H. He, "Few-layer MoS$_2$ with high broadband photogain and fast optical switching for use in harsh environments," ACS Nano **7**, 3905–3911 (2013).
3. A. Li, J. Zhang, J. C. Qiu, Z. H. Zhao, C. Wang, C. J. Zhao, and L. Hong, "A novel aptameric biosensor based on the self-assembled DNA-WS$_2$ nanosheet architecture," Talanta **163**, 78–84 (2017).
4. F. Xia, H. Wang, D. Xiao, M. Dubey, and A. Ramasubramaniam, "Two-dimensional material nanophotonics," Nat. Photonics **8**, 899–907 (2014).
5. S. Ratha and C. S. Rout, "Supercapacitor electrodes based on layered tungsten disulfide-reduced graphene oxide hybrids synthesized by a facile hydrothermal method," ACS Appl. Mater. Interfaces **5**, 11427–11433 (2013).
6. Y. C. Wang, J. Z. Ou, A. Chrimes, B. Carey, T. Daeneke, M. M. Alsaif, M. Mortazavi, S. Zhuiykov, N. Medhekar, M. Bhaskaran, J. R. Friend, M. S. Strano, and K. Kalantar-Zadeh, "Plasmon resonances of highly doped two-dimensional MoS$_2$," Nano Lett. **15**, 883–890 (2015).
7. X. J. Cai, W. Gao, L. L. Zhang, M. Ma, T. Z. Liu, W. X. Du, Y. Y. Zheng, H. R. Chen, and J. L. Shi, "Enabling prussian blue with tunable localized surface plasmon resonances: simultaneously enhanced dual-mode imaging and tumor photothermal therapy," ACS Nano **10**, 11115–11126 (2016).
8. W. J. Schutte, J. L. de Boer, and F. Jellinek, "Crystal structures of tungsten disulfide and diselenide," J. Solid State Chem. **70**, 207–209 (1987).
9. V. Q. Bui, T. T. Pham, D. A. Le, C. M. Thi, and H. M. Le, "A first-principles investigation of various gas (CO, H$_2$O, NO, and O$_2$) absorptions on a WS$_2$ monolayer: stability and electronic properties," J. Phys. **27**, 305005 (2015).
10. B. J. Carey, T. Daeneke, E. P. Nguyen, Y. C. Wang, J. Z. Ou, S. Zhuiykov, and K. Kalantar-Zadeh, "Two solvent grinding sonication method for the synthesis of two-dimensional tungsten disulphide flakes," Chem. Commun. **51**, 3770–3773 (2015).
11. A. S. Pawbake, R. Waykar, D. J. Late, and S. R. Jadkar, "Highly transparent wafer scale synthesis of crystalline WS$_2$ nanoparticle thin film for photodetector and humidity sensing applications," ACS Appl. Mater. Interfaces **8**, 3359–3365 (2016).
12. M. O'Brien, K. Lee, R. Morrish, N. C. Berner, N. Mcevoy, C. A. Wolden, and G. S. Duesberg, "Plasma assisted synthesis of WS$_2$ for gas sensing applications," Chem. Phys. Lett. **615**, 6–10 (2014).
13. J. Chen, C. J. Gao, A. K. Mallik, and H. D. Qiu, "A WS$_2$ nanosheet-based nanosensor for the ultrasensitive detection of small molecule–protein interaction *via* terminal protection of small molecule-linked DNA and Nt. BstNBI-assisted recycling amplification," J. Mater. Chem. B **4**, 5161–5166 (2016).
14. H. Y. Guan, K. Xia, C. Y. Chen, Y. H. Luo, J. Y. Tang, H. H. Lu, J. H. Yu, J. Zhang, Y. C. Zhong, and Z. Chen, "Tungsten disulfide wrapped on micro fiber for enhanced humidity sensing," Opt. Mater. Express **7**, 1686–1696 (2017).
15. E. E. Bedford, J. Spadavecchia, C. M. Pradier, and F. X. Gu, "Surface plasmon resonance biosensors incorporating gold nanoparticles," Macromol. Biosci. **12**, 724–739 (2012).
16. A. Shalabney and I. Abdulhalim, "Sensitivity-enhancement methods for surface plasmon sensors," Laser Photon. Rev. **5**, 571–606 (2011).
17. F. Zou, B. P. Wu, X. X. Wang, Y. Y. Chen, K. Koh, K. M. Wang, and H. X. Chen, "Signal amplification and dual recognition strategy for small-molecule detection by surface plasmon resonance based on calixarene crown ether-modified gold nanoparticles," Sens. Actuators B **241**, 160–167 (2017).
18. L. Guo, J. A. Jackman, H. H. Yang, P. Chen, N. J. Cho, and D. H. Kim, "Strategies for enhancing the sensitivity of plasmonic nanosensors," Nano Today **10**, 213–239 (2015).
19. S. W. Zeng, X. Yu, W. C. Law, Y. Zhang, R. Hu, X. Q. Dinh, H. P. Ho, and K. T. Yong, "Size dependence of Au NP-enhanced surface plasmon resonance based on differential phase measurement," Sens. Actuators B **176**, 1128–1133 (2013).
20. X. Cui, Y. Huang, J. Wang, L. Zhang, Y. Rong, W. Lai, and T. Chen, "A remarkable sensitivity enhancement in a gold nanoparticle-based lateral flow immunoassay for the detection of *Escherichia coli* O157:H7," RSC Adv. **5**, 45092–45097 (2015).
21. K. S. Lee, M. Lee, K. M. Byun, and I. S. Lee, "Surface plasmon resonance biosensing based on target-responsive mobility switch of magnetic nanoparticles under magnetic fields," J. Mater. Chem. **21**, 5156–5162 (2011).
22. A. Shalabaney and I. S. Abdulhalim, "Surface plasmon sensor with enhanced sensitivity using top nano dielectric layer," J. Nanophoton. **3**, 231–249 (2009).
23. R. Tabassum and B. D. Gupta, "Influence of oxide overlayer on the performance of a fiber optic SPR sensor with Al/Cu layers," IEEE J. Sel. Top. Quantum Electron. **23**, 1–8 (2016).
24. S. Singh and B. D. Gupta, "Simulation of a surface plasmon resonance-based fiber-optic sensor for gas sensing in visible range using films of nanocomposites," Meas. Sci. Technol. **21**, 115202 (2010).
25. L. Touahir, J. Niedziółka-Jönsson, E. Galopin, R. Boukherroub, A. C. Gouget-Laemmel, L. Solomon, M. Petukhov, J. N. Chazalviel, F. Ozanam, and S. Szunerits, "Surface plasmon resonance on gold and silver films coated with thin layers of amorphous silicon–carbon alloys," Langmuir **26**, 6058–6065 (2010).
26. X. Luo, T. Qiu, W. Lu, and Z. Ni, "Plasmons in graphene: recent progress and applications," Mater. Sci. Eng. R **74**, 351–376 (2013).

27. W. Wei, P. Jin, N. Y. Zhu, W. Gui, N. Zhang, S. Q. Wang, N. Luo, G. L. Chen, C. J. Lan, and Y. C. Huang, "Graphene/Au-enhanced plastic clad silica fiber optic surface plasmon resonance sensor," Plasmonics **13**, 483–491 (2018).

28. P. Subramanian, F. Barkabouaifel, J. Bouckaert, N. Yamakawa, R. Boukherroub, and S. Szunerits, "Graphene-coated surface plasmon resonance interfaces for studying the interactions between bacteria and surfaces," ACS Appl. Mater. Interfaces **6**, 5422–5431 (2014).

29. Q. L. Ouyang, S. W. Zeng, L. Jiang, L. Y. Hong, G. X. Xu, X. Q. Dinh, J. Qian, S. He, J. L. Qu, C. Philippe, and K. T. Yong, "Sensitivity enhancement of transition metal dichalcogenides/silicon nanostructure-based surface plasmon resonance biosensor," Sci. Rep. **6**, 28190 (2016).

30. A. Berkdemir, H. R. Gutiérrez, A. R. Botelloméndez, N. Perealópez, A. L. Elías, C. Chia, B. Wang, V. H. Crespi, F. López-Urías, J. C. Charlier, H. Terrones, and M. Terrones, "Identification of individual and few layers of WS$_2$ using Raman spectroscopy," Sci. Rep. **3**, 1755 (2013).

31. N. F. Chiu and T. Y. Huang, "Sensitivity and kinetic analysis of graphene oxide-based surface plasmon resonance biosensors," Sens. Actuators B **197**, 35–42 (2014).

32. A. Zavabeti, J. Z. Ou, B. J. Carey, N. Syed, R. Orrell-Trigg, E. L. H. Mayes, C. L. Xu, O. Kavehei, A. P. O'Mullane, R. B. Kaner, and K. Kalantar-Zadeh, "A liquid metal reaction environment for the room-temperature synthesis of atomically thin metal oxides," Science **358**, 332–335 (2017).

33. B. J. Carey, J. Z. Ou, R. M. Clark, K. J. Berean, A. Zavabeti, A. S. R. Chesman, S. P. Russo, D. W. M. Lau, Z. Q. Xu, Q. L. Bao, O. Kevehei, B. C. Gibson, M. D. Dickey, R. B. Kaner, T. Daeneke, and K. Kalantar-Zadeh, "Wafer-scale two-dimensional semiconductors from printed oxide skin of liquid metals," Nat. Commun. **8**, 14482 (2017).